5th US Combustion Meeting
Organized by the Western States Section of the Combustion Institute
and Hosted by the University of California at San Diego
March 25-28, 2007

A computational investigation of sooting limits of spherical diffusion flames

V.R. Lecoustre[1], B.H. Chao[2], P.B. Sunderland[1], D.L. Urban[3], D.P. Stocker[3] and R.L. Axelbaum[4]

[1]*Dept. of Fire Protection Engineering, Univ. of Maryland, College Park, MD 20742, USA*

[2]*Dept. of Mechanical Engineering, Univ. of Hawaii, Honolulu, HI 96822, USA*

[3]*NASA Glenn Research Center, Cleveland, OH 44135, USA*

[4]*Dept. of Mechanical and Aerospace Engineering, Washington Univ., St. Louis, MO 63130, USA*

Limiting conditions for soot particle inception in spherical diffusion flames were investigated numerically. The flames were modeled using a one-dimensional, time accurate diffusion flame code with detailed chemistry and transport and an optically thick radiation model. Seventeen normal and inverse flames were considered, covering a wide range of stoichiometric mixture fraction, adiabatic flame temperature, and residence time. These flames were previously observed to reach their sooting limits after 2 s of microgravity. Sooting-limit diffusion flames with residence times longer than 200 ms were found to have temperatures near 1190 K where C/O = 0.6, whereas flames with shorter residence times required increased temperatures. Acetylene was found to be a reasonable surrogate for soot precursor species in these flames, having peak mole fractions of about 0.01.

1. Introduction

Formation of soot in combustion is an active research topic, as discussed in the reviews of [1-3]. One fundamental measure of flame sooting behavior is sooting limits. Sooting limits of spherical microgravity diffusion flames were observed by Sunderland et al. [4]. The present work is an investigation into those flames with the aid of a detailed computational model.

In the past, most data on fundamental sooting limits came from studies of laminar premixed flames [1,2,5-8]. One reason for this is that both temperature and carbon-to-oxygen atom ratio, C/O, are nearly constant in the soot-forming regions of premixed flames. Past studies found sooting limits in premixed flames to arise from a competition between fuel pyrolysis and oxidation of soot precursors [8]. It was found that soot inception in premixed flames cannot occur when C/O is below a critical value, about 0.6 for ethylene [1,2,5,7,8].

A similar competition can occur in diffusion flames on the fuel side owing to the presence of oxygen in species such as CO_2 and H_2O [4,9]. Du et al. [9] showed that adding CO_2 to the fuel side of diffusion flames can suppress soot formation chemically. Despite the differences between soot inception in premixed and nonpremixed flames, the C/O atom ratio has been shown to be relevant to sooting limits in diffusion flames [4,10]. Past experimental work on spherical

diffusion flames in microgravity supported a critical local C/O value of about 0.6 for ethylene [4].

Temperature plays a different role in premixed and nonpremixed flames: increasing temperature suppresses soot formation in premixed flames, whereas it enhances soot formation in nonpremixed flames [2,8]. Previous research on diffusion flames has identified an onset temperature at which soot particles are first observed to be in the range of 1250 – 1650 K [2,11-14].

In addition to C/O ratio and temperature, residence time (or strain rate) is the third parameter critical to soot inception limits. Soot induction times of 0.8 – 15 ms were reported by Tesner and Shurupov [15] for acetylene/nitrogen mixtures at 1473 K. Strain rates of 30 – 200 s^{-1} were observed to prevent soot formation in counterflow diffusion flames [16,17].

Microgravity allows the observation of strain-free diffusion flames. It also allows conditions with much longer residence times than can be obtained in normal gravity. These long residence times can yield new insights into soot inception limits, but they cause increased radiative losses that require consideration.

This study seeks to further investigate the effects of local C/O atom ratio, local temperature, and residence time on sooting limits of spherical diffusion flames. The flames under consideration are the 17 microgravity flames of Sunderland et al. [4], having both normal and inverse convection directions and disparate stoichiometric mixture fraction, adiabatic temperature, and residence time. The model used here is a one-dimensional, time accurate diffusion flame code with detailed chemistry and transport and an optically thick radiation model.

2. Numerical

The conservation equations were solved numerically using a flame code that includes detailed kinetic and transport properties. The numerical code was modified from the Sandia burner-stabilized PREMIX [18] code, which was originally developed for the study of one-dimensional freely propagating and burner-stabilized premixed laminar flames. The code was adapted for spherical diffusion flames allowing for optically thick radiative heat losses, as described in [19]. Both steady state and transient flames can be modeled.

Conservation of mass, energy, and gas species for this problem are:

$$\frac{\partial \rho}{\partial t} + \frac{1}{r^2}\frac{\partial (r^2 \rho u)}{\partial r} = 0 \qquad (1)$$

$$\rho c_p \frac{\partial T}{\partial t} = \frac{1}{r^2}\frac{\partial}{\partial r}(r^2 \lambda \frac{\partial T}{\partial r}) - \rho u c_p \frac{\partial T}{\partial r} - \sum_{k=1}^{K}(\rho c_{p,k} Y_k V_k \frac{\partial T}{\partial r} + h_k \omega_k Y_k) - Ra \qquad (2)$$

$$\rho \frac{\partial Y_k}{\partial t} = -\frac{1}{r^2}\frac{\partial}{\partial r}\left(r^2 \rho Y_k V_k\right) - \rho u \frac{\partial Y_k}{\partial r} + W_k \omega_k Y_k \qquad , \text{k} = 1, 2, \ldots, \text{K} , \qquad (3)$$

where T is temperature, Y_k is mass fraction of species k, W_k is molecular weight of species k, t is time, r is radial spatial coordinate, u is radial flow velocity, ρ is gas density, c_p is averaged specific heat at constant pressure, λ is heat conductivity, h_k is specific enthalpy of species k, $c_{p,k}$

is specific heat of species k, V_k is diffusion velocity of species k, ω_k is production rate of species k, K is number of species, and Ra is rate of radiative heat loss. The equations were solved subject to the following boundary conditions:

$$r = r_b : T = T_b; Y_k(u + V_k) = uY_{k,b}, k = 1,2...N \quad (4)$$

$$r \to +\infty : T \to T_\infty; Y_k \to Y_{k,\infty}, k = 1,2...N \quad (5)$$

where subscripts b and ∞ refer to conditions at the burner surface and at the ambient, respectively. Variable $Y_{k,b}$ is the value of the k^{th} species mass fraction within the flow at the burner outlet, matching the value supplied as an input. Because drop tower experiments did not show a significant increase in burner surface temperature [19], T_b was taken to be constant.

The computation requires a set of initial conditions that resemble the ignition process. Following the approach adopted by Tse et al. [20], the initial (ignition) conditions were prescribed as the steady-state solution of the same flame but without radiation, assuming adiabatic conditions at the burner exit, and in a compressed domain to approximate the ignition conditions of the experiments. The compressed domain was chosen to extend 1.2 cm from the burner center. The outer boundary temperature was forced to remain at the ambient temperature of 295 K. The steady-state computations begin with a set of prescribed initial distributions of grid points, temperature, species concentrations, and an estimate of the location and thickness of the reaction region. Once the steady-state solution is obtained, the grid is adapted to reduce the gradients and curvature and to improve the accuracy. New grid points are added until all values of the gradients and curvature are below the user specified limits, and further addition of grid points does not affect the solution.

The steady state solution on the compressed domain is then used as the initial condition of the transient computations by expanding the domain of computation to 100 cm from the center of the burner, by adding grids point to fill the gap between the compressed and normal domains. All the computations used a grid of about 200 mesh points, finer in the area of high gradients (flame location), becoming coarser close to the outer boundary. Test cases were run to insure grid independence. Typically, about 120 extra mesh points were added from the compressed to the extended computation domain. The initial conditions at those extra mesh points were taken to be the user specified values for the outer boundary.

For the transient computation of the flame structure, radiative losses were considered. Radiation was considered optically thick and caused only by the participation of CO_2, H_2O, and CO. The radiative properties of these gases were formulated by a statistical narrow-band model with a spectral bandwidth of 25 cm^{-1}. The emissivities were extracted from the line by-line values given by the HITRAN database [23].

3. Experimental

The tests considered here were performed and reported in [4]. Further details of the apparatus are contained in [21]. These experiments were conducted in microgravity in the NASA Glenn 2.2 s drop tower. The burner was a 6.4 mm diameter porous stainless steel sphere. All tests were conducted in quiescent ambient gas at 295 K and 0.98 bar and ignition was performed in microgravity. The tests employed three gases: ethylene, nitrogen, and oxygen. A color video camera was used to image the flames.

A summary of the 17 sooting limit flames of [4] is given in Table 1. Burner flow rates were selected such that all flames involved a steady-state ethylene consumption rate of 1.51 mg/s, assuming complete combustion. Normal and inverse conditions are denoted by environments of oxidizer and fuel, respectively. Normal flames are realized when fuel discharges from the burner into an oxidizer atmosphere, while inverse flames are realized when oxidizer flows from the burner into an atmosphere of fuel. The fuel and oxygen mole fractions in the supply gases, $X_{C2H4,0}$ and $X_{O2,0}$, vary widely. This yielded a wide range of stoichiometric mixture fraction, Z_{st}, as shown. Adiabatic flame temperatures were calculated using Chemical Equilibrium with Applications, CEA [22].

Residence time is defined here as the mass of gas contained between the flame and the burner surface divided by the burner mass flow rate [4]. This characterizes the time required for a parcel of gas to convect from the burner surface to the flame sheet.

Table 1: Summary of the sooting limit flames, reproduced from [4].

Flame	Environment	$X_{C2H4,0}$	$X_{O2,0}$	Zst	t_{res}, s	T_{ad}, K
1	Oxidizer	1	0.22	0.065	2.06	2390
2	Oxidizer	0.6	0.21	0.102	1.44	2326
3	Oxidizer	0.31	0.21	0.18	1.03	2226
4	Oxidizer	0.25	0.23	0.225	0.86	2238
5	Oxidizer	0.18	0.28	0.333	0.429	2306
6	Oxidizer	0.17	0.29	0.353	0.383	2308
7	Oxidizer	0.11	0.5	0.586	0.107	2381
8	Oxidizer	0.11	0.8	0.685	0.038	2528
9	Oxidizer	0.15	1	0.661	0.015	2740
10	Fuel	1	0.13	0.041	0.024	1847
11	Fuel	0.8	0.13	0.051	0.039	1835
12	Fuel	0.6	0.13	0.066	0.049	1814
13	Fuel	0.21	0.25	0.277	0.196	2274
14	Fuel	0.19	0.3	0.336	0.197	2370
15	Fuel	0.15	0.5	0.509	0.283	2539
16	Fuel	0.12	0.8	0.666	0.374	2578
17	Fuel	0.13	1	0.692	0.406	2670

4. Results

The 17 spherical diffusion flames summarized in Table 1 were simulated using the modified PREMIX code. Predictions at 2 s after ignition were emphasized to better understand the conditions associated with the observed sooting limits. The flames modeled covered both normal and inverse configurations for a wide range of residence time, stoichiometric mixture fraction, and adiabatic flame temperature.

The wide range of residence times for the 17 flames, 0.015 – 2.06 s, has important implications for sooting limits. At long residence times sooting limits are not expected to depend on residence time. However short residence times could prevent soot formation [15-17]. Thus it is instructive to first consider pairs of flames with similar residence times but with different Z_{st}. Two such pairs are flames 5 and 17, which have residence times near 400 ms, and flames 8 and 11, which have residence times near 40 ms.

Flames 5 and 17, which are sooting limit flames with long residence times, are considered in Fig. 1. This plot shows predicted temperatures, C/O ratios, and C_2H_2 mole fraction profiles. Whereas these flames have similar residence times, flame 5 is a normal flame with Z_{st} = 0.333 and flame 17 is an inverse flame with Z_{st} = 0.692. The locations of peak temperature here agree with measured flame radii from [4]. The peak temperature of flame 17 is 200 K higher than that of flame 5, supporting the finding of [4] that increased Z_{st} favors soot-free conditions.

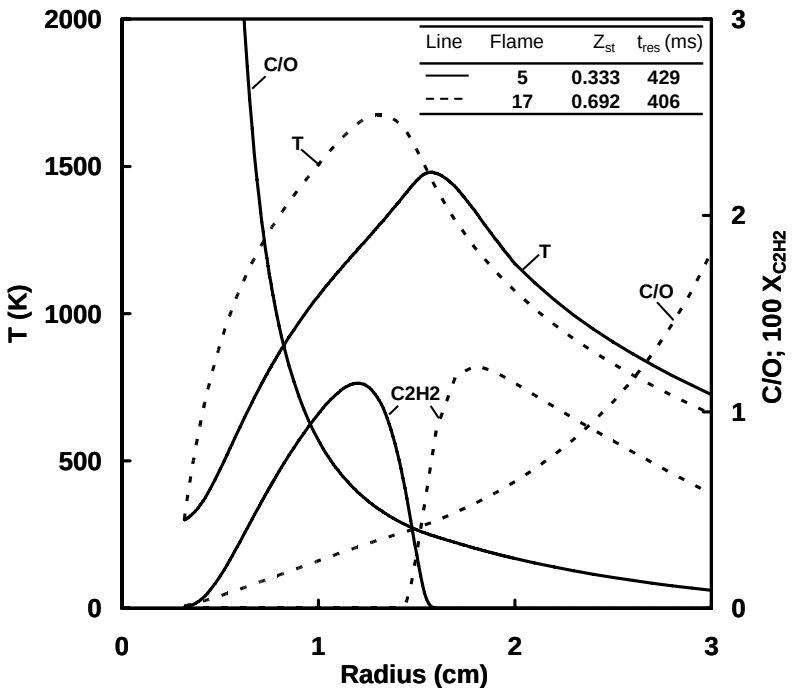

Figure 1: Predicted radial profiles of *T*, C/O ratio and X_{C2H2} at 2 s after ignition for two sooting limit flames with long residence times.

Figure 1 reveals that for flames 5 and 17, each has a region on the fuel side where C/O is about 0.6 and T is about 1300 K. Past work [4] proposed this to be the case for all sooting limit flames with sufficiently long residence times.

The present model is based on GRI-Mech 3.0 and does not include soot kinetics. However C_2H_2 chemistry is included and C_2H_2 is used here as a surrogate for soot precursor species [6]. Fig. 1 shows X_{C2H2} profiles for flames 5 and 17. The results suggest that sooting limit flames with long residence times have peak values of X_{C2H2} of about 0.01. Additionally the peak acetylene mole fractions for both flames are predicted to occur on the fuel side where C/O is about 0.6 and *T* is about 1300 K. This is near where the analysis of [4] predicts the first soot to appear.

A plot similar to that of Fig. 1 is shown for flames 8 and 11 in Fig. 2. These sooting limit flames have relatively short residence times, about an order of magnitude shorter than the flames of Fig. 1. Flame 8 is a normal flame with Z_{st} = 0.685 and flame 11 is an inverse flame with Z_{st} = 0.051. The locations of peak temperature here agree with measured flame radii from [4]. The peak temperature of flame 8 is 400 K higher than that of flame 11, again supporting that increased Z_{st} favors soot-free conditions.

Figure 2 reveals that for flames 8 and 11, each has a region on the fuel side where C/O is about 0.6 and *T* is about 1400 K. This increased temperature is attributed to the decreased residence times of these flames.

Figure 2 also shows X_{C2H2} profiles for flames 8 and 11. The results suggest that when residence time is short, sooting limit flames have increased peak values of X_{C2H2}, here about 0.02 for both flames. The location of peak acetylene mole fraction vis-à-vis *T* and C/O ratio remains under investigation for flame 11.

The temperature profiles of Figs. 1 and 2 are plotted versus C/O ratio in Fig. 3. For all four flames, temperature peaks near C/O = 1/3, reflecting the stoichiometry of ethylene-oxygen combustion. Of primary interest here is the temperature on the fuel side of each flame where C/O ratio is 0.6. The flames with long residence times (flames 5 and 17) have temperatures of about 1300 K at this location. In contrast, the flames with short residence times (flames 8 and 11) have temperatures of about 1400 K here. Higher temperatures are required to offset the shorter residence times here.

The effects of residence time on the temperature required for soot formation is now examined using predictions for all 17 flames of Table 1. Figure 4 shows the predicted fuel-side temperatures at the locations of C/O = 0.6. These are plotted versus residence time.

Figure 4 reveals that for long residence times these temperatures are similar, while for short residence times increased temperatures are required for soot formation. The data of Fig. 4 suggests, for the present flames, that short and long residence times vis-à-vis soot inception are those less than 110 ms and longer than 200 ms, respectively. Note that these flames involve over two orders of magnitude variation in residence time.

The data of Fig. 4 show

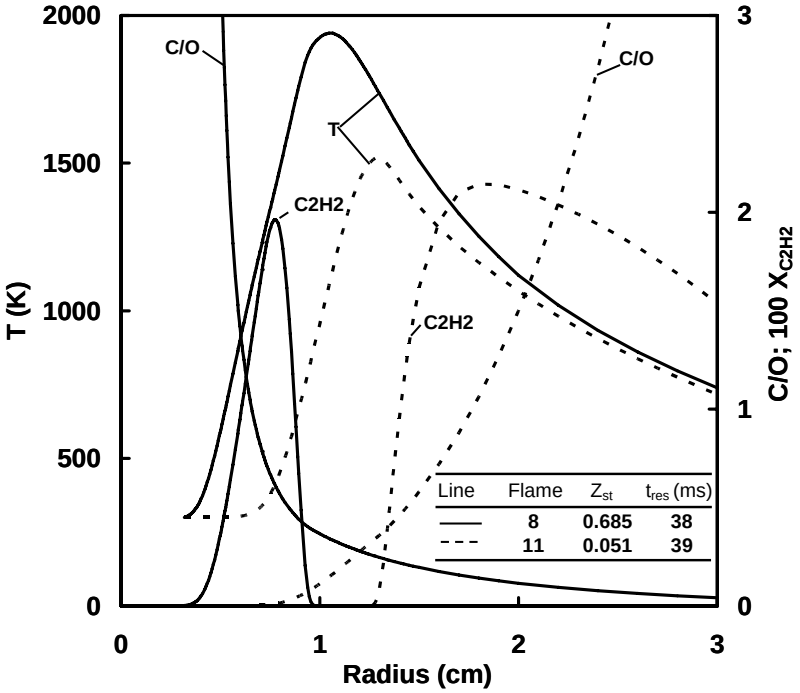

Figure 2: Predicted radial profiles of *T*, C/O ratio and X_{C2H2} at 2 s after ignition for two sooting limit flames with short residence times.

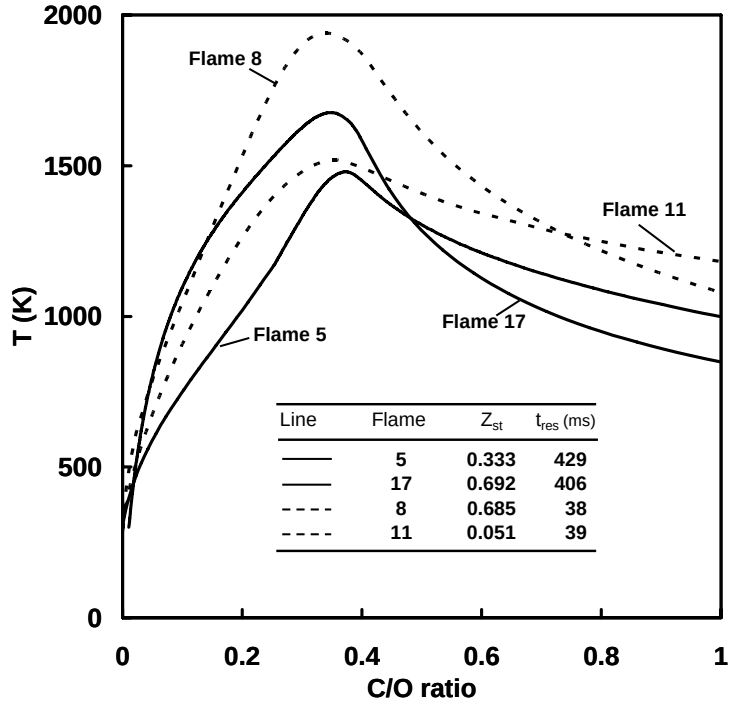

Figure 3: Predicted temperatures as a function of C/O at 2 s after ignition for sooting limit flames with long residence times (solid curves) and with short residence times (dashed curves).

interesting trends with respect to residence time. The possibility of trends with respect to stoichiometric mixture fraction are examined in Fig. 5. Here the temperature data of Fig. 4 are replotted with an abscissa of Z_{st}.

For flames with long residence times, Fig. 5 shows that the temperature at the expected location of soot inception is not strongly dependent on Z_{st}. For these flames, sooting limit conditions occur when the fuel-side temperature is about 1190 K at locations with C/O = 0.6. This finding applies for both normal and inverse flames across wide ranges of Z_{st} and T_{ad}. On the other hand, when residence time is short, soot formation requires increased temperatures.

5. Conclusions

Computations (with detailed chemistry and transport) of spherical diffusion flames at sooting limits have been performed. Seventeen flames were considered, these having been previously observed to reach sooting limits after 2 s of microgravity. The key findings are as follows:

1) Sooting-limit diffusion flames with sufficiently long residence times have similar fuel-side temperatures where C/O = 0.6. For flames with residence times above 200 ms these temperatures average 1190 K and are not affected by Z_{st}.
2) Flames with residence times shorter than 110 ms require increased temperatures at this location.
3) Acetylene is a reasonable surrogate for soot precursor species in these flames. Peak acetylene mole fractions of about 0.01 are predicted at the sooting limits.

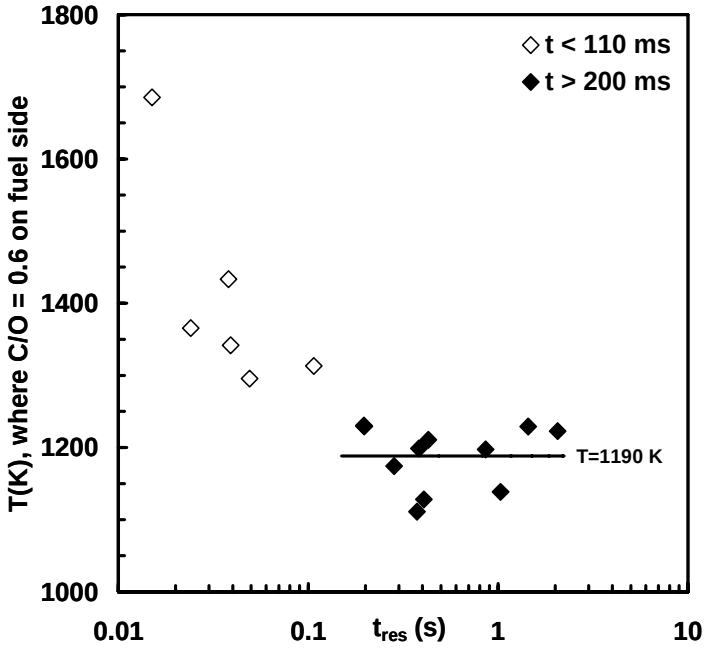

Figure 4: Predicted fuel-side temperatures where C/O = 0.6 as a function of residence time at 2 s after ignition for the 17 flames of Table 1.

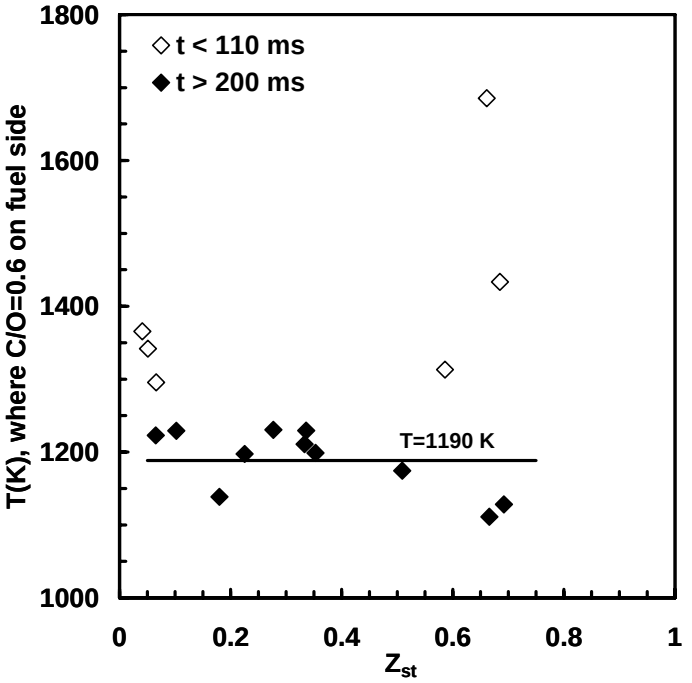

Figure 5: Predicted fuel-side temperatures where C/O = 0.6 as a function of stoichiometric mixture fraction at 2 s after ignition for the 17 flames of Table 1.

Acknowledgments

This work was supported by NASA Grants NCC3-696 and NAG3-1912 (BHC), NNC05-AA46A (PBS), and NCC3-697 and NAG3-1910 (RLA). Discussions with S.A. Skeen were very helpful.

References

[1] B.S. Haynes, H.G. Wagner, Soot formation, *Prog. Energy Combust.* Sci. 7 (1981), 229.
[2] I. Glassman, Soot formation in combustion processes, *Proc. Combust. Inst.,* 22 (1988), 295.
[3] D.L. Urban, G.M. Faeth, Soot research in combustion science: introduction and review of current work, *39th AIAA Meeting*, January 8-11, Reno, NV, AIAA 2001-0332.
[4] P.B. Sunderland, D. L. Urban, D.P. Stocker, B.H. Chao, R.L. Axelbaum, Sooting limits of microgravity spherical diffusion flames in oxygen-enriched air and diluted fuel, *Combust. Sci. Technol*.,176 (2004), 2143.
[5] M.M. Harris, G.B. King, N.M. Laurendeau, Influence of temperature and hydroxyl concentration on incipient soot formation in premixed flames, *Combust. flame*, 64 (1986), 99.
[6] P. Markatou, H. Wang, M. Frenklach, A computational study of sooting limits in laminar premixed flames of ethane, ethylene and acethylene, *Combust. flame*, 93 (1993), 467.
[7] F. Takahashi, Sooting correlations for premixed combustion. In Dryer, F.L. and Sawyer, R.F. (Eds.*). Physical and Chemical Aspects of Combustion: A Tribute to Irvin Glassman*, Gordon and Breach, Amsterdam 1997, pp. 161–187.
[8] F. Takahashi, I. Glassman, Sooting correlations for premixed flames. *Combust. Sci. Technol.* 37 (1984), 1.
[9] D.X. Du, R.L. Axelbaum, C.K. Law, The influence of carbon dioxide and oxygen as additives on soot formation in diffusion flames, *Proc. Combust. Inst.*, 23 (1990), 1501.
[10] J. Du, R.L. Axelbaum, The effect of flame structure on soot-particle inception in diffusion flames, *Combust. Flame*, 100 (1995), 367.
[11] R.A. Dobbins, Soot inception temperature and the carbonization rate of precursor particles, *Combust. Flame*, 130 (2002), 204.
[12] I. Glassman, Sooting laminar diffusion flames: effect of dilution, additives, pressure, and microgravity, *Proc. Combust. Inst*., 27 (1998), 1589.
[13] R.J. Santoro, T.T. Yeh, J.J. Horvath, H.G. Semerjian, The transport and growth of soot particles in laminar diffusion flames, *Combust. Sci. Technol.*, 53 (1987), 89.
[14] P.B. Sunderland, G.M. Faeth, Soot formation in hydrocarbon air laminar jet diffusion flames, *Combust. Flame*, 105 (1996), 132.
[15] P.A. Tesner, S.V. Shurupov, Soot formation from acetylene-benzene mixture, *Combust. Sci. Technol.*, 92 (1993), 71.
[16] D.X. Du, R.L. Axelbaum, C.K. Law, Experiments on the sooting limits of aerodynamically-strained diffusion flames, *Proc. Combust. Inst.*, 22 (1988), 387.
[17] K.-C. Lin, G.M. Faeth, Effects of hydrodynamics on soot formation in laminar opposed-jet diffusion flames, *J. Propul. Power*, 12 (1996), 691.
[18] R.J. Kee, J.F. Grear, M.D. Smooke, J.A. Miller, E. Meeks, A program for modeling steady, laminar, one-dimensional premixed flames, *Sandia National Laboratories Report* No. SAND85-8240 1987.
[19] K.J. Santa, B.H. Chao, P.B. Sunderland, J.L. Taylor, D.L. Urban, D.P. Stocker, R.L. Axelbaum, Radiative extinction of gaseous spherical diffusion flames in microgravity, *44th AIAA Meeting*, January 8-11, Reno, NV, AIAA 2006-747.
[20] S.D. Tse, D. Zhu, C.-J. Sung Y. Ju, C.K. Law, Microgravity burner generated spherical diffusion flames experiment and computation, *Combust. Flame*, 125 (2001), 1265-1278.
[21] Sunderland, P.B., Axelbaum, R.L., Urban, D.L., Chao, B.H., Liu, S., Effects of structure and hydrodynamics on the sooting behavior of spherical microgravity diffusion flames, *Combust. Flame*, 132 (2003), 25.
[22] B.J. McBride and S. Gordon, *Computer Program for Calculation of Complex Chemical Equilibrium Compositions and Applications*, NASA RP-1311-P2 (1996), Cleveland, OH.
[23] L.S. Rothman, C.P. Rinsland, A. Goldman, S.T. Massie, D.P. Edwards, J.-M. Flaud, A. Perrin, C. Camy-Peyret, V. Dana, J.-Y. Mandin, J. Schroeder, A. Mccann, R.R. Gamache, R.B. Wattson, K. Yoshino, K.V. Chance, K.W. Jucks, L.R. Brown, V. Nemtchinov, P. Varanasi, J. Quant. Spectrosc. Radiat. Transf. 82 (2003) 5-44.